

1 **Improving Aboveground Biomass Estimates with 3D Tree Crown Parameters from** 2 **UAV-LS in Beech Forests**

3 *Nicola Puletti^{a,*}, Simone Innocenti^a, Matteo Guasti^a, Cesar Alvites^b, Carlotta Ferrara^c*

4 ^aCREA, Research Centre for Forestry and Wood, Viale Santa Margherita 80, Arezzo, IT-52100

5 ^bUniversity of Molise, Department of Agricultural, Environmental and Food Sciences, Via De Sanctis
6 1, Campobasso, IT-86100

7 ^cCREA, Research Centre for Forestry and Wood, Via Valle della Quistione, Roma, IT-00166

8 *Corresponding author: nicola.puletti@crea.gov.it

9 10 **Abstract**

11 Accurate estimates of aboveground biomass (AGB) are essential for forest policies to reduce carbon
12 emissions. Unmanned aerial laser scanning (UAV-LS) offers unprecedented millimetric detail but is
13 underutilized in monitoring broadleaf Mediterranean forests compared to coniferous ones. This study
14 aims to design and evaluate a procedure for AGB estimates based on the predictive power of crown
15 features. In a first phase, we manually defined Quantitative Structure Models (QSMs) for 320 trees
16 using UAV-LS, ALS, and co-registered terrestrial laser scanning (TLS) data, providing the best non-
17 destructive AGB reference in the absence of destructive measurements. For each reference tree we also
18 measured crown projection and crown volume to build two separated models relating AGB to such
19 crown features. In a second phase we evaluated the potential of UAV-LS for quantifying AGB in a
20 pure European beech (*Fagus sylvatica*) forest and compared it with traditional ALS estimates, using
21 full automatic procedures. The two obtained tree-level AGB models were then tested using three
22 datasets derived from 35 sampling plots over the same study area: (a) 1130 trees manually segmented
23 (phase-2 reference); (b) trees automatically extracted from ALS data; and (c) trees automatically
24 extracted from UAV-LS data. Results demonstrate that detailed UAV-LS data improve model
25 sensitivity compared to ALS data (RMSE = 45.6 Mg ha⁻¹, RMSE% = 13.4%, R² = 0.65, for the best
26 ALS model; RMSE = 44.0 Mg ha⁻¹, RMSE% = 12.9%, R² = 0.67, for the best UAV-LS model),
27 allowing for the detection of AGB differences even in quite homogenous forest structures. Overall, this
28 study demonstrates that combining different laser scanner data can foster non-destructive AGB
29 estimation in forested areas across hectare scales (1 to 100 ha).

30 *Keywords: Biomass, LiDAR, Tree allometric scaling rules, Temperate forests, Forest mensuration*

32 **1. Introduction**

33 Forests are fundamental natural carbon sinks, actively contributing to mitigating climate change
34 (Verkerk et al. 2019). In recent decades, the demand for accurate methods to estimate aboveground
35 biomass (AGB) in forest ecosystems has grown due to its crucial role in the carbon cycle and in
36 assessing forest health status, habitat quality, forest disturbance and restoration (Heinrich et al. 2021).
37 Carbon stock estimates in forest ecosystems are strictly linked to AGB, which varies with eco-
38 physiological, environmental, and management stand-based factors.

39 General scaling rules for metabolic and structural plant allometry, such as the theory of Euclidean
40 geometric scaling or metabolic scaling theory (MST (Owen, Flynn, and Lines 2021)), provide valuable
41 insights into biomass patterns at broad scales. However, these theories assume a constant tree crown-
42 volume relation for all the trees of a given species, even though the variability in crown structure,
43 rather than constancy, is crucial for a tree's success in crowded conditions (Pretzsch and Dieler 2012).
44 Therefore, developing models tailored to specific local conditions is essential for managers and
45 practitioners to address site-specific management challenges and achieve their objectives (Ploton et al.
46 2020; Xu et al. 2021).

47 One of the major limitations affecting local allometric model accuracy is the reduced number of
48 calibration samples, which typically require destructive harvesting. This process can be costly when
49 used through traditional tools like chainsaws, callipers, and measuring tape, and it often prevents large
50 trees from being harvested (Calders et al. 2022). In addition, during the felling phase, the tree crown is
51 subjected to breakages, leading to inaccurate measurements.

52 Terrestrial Laser Scanning (TLS) is widely recognized as one of the most accurate and non-destructive
53 methods for estimating individual tree AGB (Brede et al. 2019; Calders et al. 2015, 2022; N. Puletti et
54 al. 2020; Pretzsch 2021). However, its application across large areas faces considerable logistical
55 challenges. TLS campaigns are time-intensive, requiring up to 3–7 days per hectare (Brede et al. 2022),
56 and demand substantial manual effort for individual tree segmentation, particularly in dense and
57 complex forest canopies. These constraints significantly limit its feasibility for calibrating and
58 validating AGB models over broad and heterogeneous landscapes.

59 Generating wall-to-wall AGB maps requires the integration of field-surveyed data with metrics
60 obtained from Laser Scanning devices, such as Airborne Laser Scanning (ALS) (Brososke et al. 2014;
61 G. Shao et al. 2018). Although ALS data have been extensively tested in forest ecosystems and are
62 today an integral part of many national-scale environmental monitoring programs (Chirici et al. 2020),
63 challenges remain in their application for AGB assessment. In particular, estimating AGB for
64 deciduous trees is more difficult than for conifers, likely due to differences in growth patterns (Næsset
65 2004). For example, Beech (*Fagus sylvatica* L.) trees, which have deliquescent tree forms, allocate a
66 great amount of biomass into lateral branches, introducing noise into the relationship between height
67 and volume/biomass. Recent studies have demonstrated that ALS data can be profitably used in such
68 stands when forest structure and species mixture have great variability, particularly if specific variables
69 like site productivity are included (G. Shao et al. 2018). Without such ancillary data, ALS models for
70 pure deciduous forests remain inaccurate (J. Shao et al. 2022; G. Shao, Fei, and Shao 2023; Cao et al.
71 2023). Despite the widespread use of ALS for AGB estimation, its application in deciduous forests,
72 such as pure beech stands, remains challenging due to the unique structural variability of these forests,
73 characterized by deliquescent branching and lateral biomass allocation.

74 The recent miniaturisation of LiDAR instruments (Z. Wang and Menenti 2021) has paved the way to
75 integrate more detailed data above the canopy (Brede et al. 2019). Laser scanners mounted on
76 Unmanned Aerial Vehicles (UAV-LS) offer a promising solution to enhance the quality of ALS-based
77 statistical allometric models in temperate and boreal forests (Nicola Puletti, Innocenti, and Guasti
78 2024), particularly in pure-broadleaved forests (Brede et al. 2019; N. Puletti et al. 2020; J. Shao et al.
79 2022, Table–A1). UAV-LS offers several advantages over traditional ALS systems (Torresan et al.
80 2017; Alvites et al. 2022). First, it provides a much higher point density (>1000 points m^{-2}), enabling
81 detailed crown reconstruction. Second, UAV-LS is highly flexible, with faster flight planning (10-20 ha
82 $hour^{-1}$) and lower costs, making it suitable for covering large forest areas efficiently.

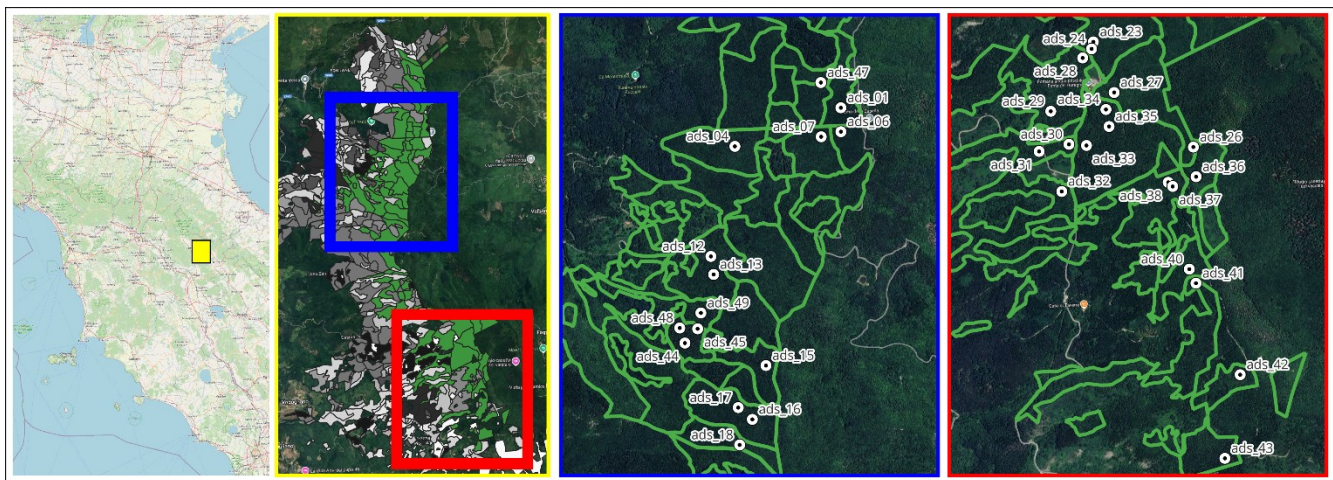
83 To address these limitations, this study evaluates how detailed crown metrics derived from UAV-LS
84 can improve the accuracy of AGB estimates in pure beech forests, leveraging precise crown feature
85 measurements and automated individual tree segmentation (ITS). This study aims to assess the
86 potential of UAV-LS in improving AGB estimates in pure beech forests by leveraging precise crown
87 feature measurements. The analysis combines TLS reference data, manually extracted crown metrics,
88 and an automated ITS algorithm to evaluate UAV-LS's effectiveness compared to ALS-based methods.
89 The experiment was conducted in managed pure beech forests characterized by homogeneous, dense

90 canopy cover and minimal differences in vertical structure, but a wide range of three diameters (i.e.,
91 diameter at breast height, dbh, ranging from 4 to 85 cm). TLS data were used as input reference data
92 for variables like tree position, dbh, and tree volume derived from quantitative structure models
93 (QSMs, Georgi et al. 2018). In the first phase, UAV-LS data were manually processed to obtain a
94 precise measure of crown features and tree volume for over 300 trees used as reference. Then, AGB
95 was derived as the product of tree volume, Biomass Expansion Factor (BEF), and Wood Basal Density
96 (WBD). Based on this, an *AGB~crown* model was developed. In the second phase, the *AGB~crown*
97 model was applied using crown features derived from an automatic ITS algorithm as predictor. Finally,
98 plot-level products obtained by ALS and UAV-LS point clouds were compared with reference data to
99 assess their performance.

100 2. Material and methods

101 2.1. Study area and data collection

102 This study was conducted in Alpe di Catenaiia, Italy (Figure 1). Terrestrial (TLS) and UAV LiDAR
103 (UAV-LS) data were collected in October-December 2023 across 12 circular sampling plots (15 m
104 radius) in pure beech forest stands with similar climate conditions, soil types, forest structure, and
105 management history (Nicola Puletti, Innocenti, and Guasti 2024).



106
107 Figure 1: Study area and sampling sites location.

108

109 TLS-inventory measurements were conducted by GeoSLAM ZEB-REVO (GeoSLAM Ltd.,
110 Ruddington, England) lightweight mobile laser scanner. It features a rotating 2D scanning device and

111 an inertial measurement unit in the handle body. The system acquires 3D information of the
 112 surrounding area using the motion provided by the scanning head on the motor drive, enabling the
 113 application of 3D simultaneous location and mapping algorithms (N. Puletti et al. 2020). This TLS
 114 requires the starting and ending points of the scan process to coincide with some overlaps during the
 115 scan path. The centre of each plot was georeferenced using an RTK GPS. Using TLS data, 320
 116 sampling trees were measured following the procedure described in Section 2.2. Forest stand
 117 characteristics are summarized in Table 1.

118 Table 1: Stand characteristics based on trees manually isolated in the Terrestrial Laser Scanning (TLS)
 119 point cloud. Volume was derived from Quantitative Structure Models (QSMs).

	min	mean (st.dev.)	max
$N\ ha^{-1}$	141.5	443.4 (239.1)	1174.2
$dbh\ (cm)$	4.0	34.9 (6.6)	85.0
$TH\ (m)$	2.9	14.1 (4.0)	26.4
$tree\ volume\ (m^3)$	152.4	282.1 (90.7)	474.8

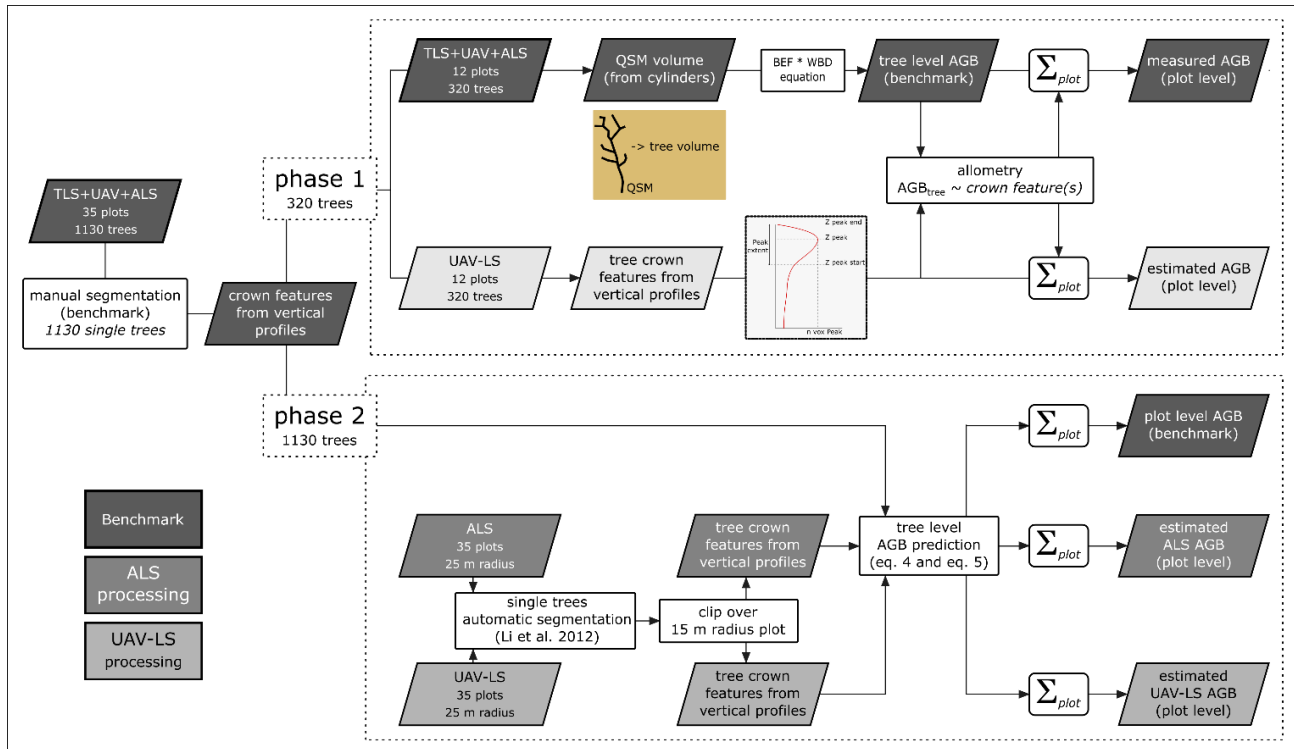
120

121 Airborne LiDar data were acquired over a 42 km² area surrounding the surveyed plots using a Riegl
 122 Q680i discrete-return sensor mounted on a Partenavia/Vulcanair P68-Victor aeroplane. The flight,
 123 performed on July 15, 2021 at an altitude of 915 m above the ground, used a 400-kHz pulse repetition
 124 rate, resulting in an average density of 25 pulses per m². LiDAR points were first classified into ground
 125 and non-ground (vegetation) using the lidR package (Roussel et al. 2020). A 1-m resolution digital
 126 terrain model raster layer was obtained by interpolating ground points to normalize the point cloud.

127 We simultaneously collected UAV-LS data and field measurements over the sampling plots. The UAV-
 128 LS LiDAR platform consisted of a DJI Matrice 350 quadcopter integrated with a Zenmuse L1 LiDAR
 129 sensor (DJI Inc. in Shenzhen, China), an advanced scanning sensor designed for aerial surveying
 130 applications. It integrates a LiDAR module, an RGB camera with a non-full-frame configuration, and
 131 an inertial measurement unit (IMU). With a detection range of 450 m under 80% reflectivity
 132 conditions, a high point rate of up to 240,000 points per second and ranging accuracy of 3 cm at a range
 133 of 100 m (Diara and Roggero 2022; Štroner, Urban, and Línková 2021), the system provides high-
 134 quality data. Flights were conducted approximately 55 m above the digital terrain model uploaded to
 135 the UAV-LS at a speed of approximately 13 h⁻¹, resulting in a mean point cloud density of more than
 136 1500 points m⁻². Data processing was carried out in Terra® which allowed the import and the

137 alignment of drone flight trajectory data. From Terra® the complete point cloud was exported in LAS
 138 format.

139 TLS, UAV-LS, and ALS data were aligned by assigning RTK GPS positions to TLS data and using
 140 Cloud Compare software (GPL software 2021; Nicola Puletti et al. 2024). The aligned three-point
 141 cloud data (TLS, UAV-LS, ALS) collected over the 12 sampling plots were clipped to the
 142 corresponding 15 m radius circles, producing a separate point cloud for each sampling plot.



143
 144 Figure 2: Processing workflow. In the first phase (upper panel) 12 sampling plots among 35 measured
 145 were processed. QSMs for more than 300 trees were obtained from manual segmentation. Vertical
 146 Profiles Features (VPFs) were derived from voxelised point clouds of each sampled tree. The outputs
 147 of this first phase are: (i) plot level AGB, used as reference for phase 2, and (ii) AGB~VPFs model. In
 148 the second phase (right panel), two fully automatic procedures were compared using UAV-LS and ALS
 149 data from all 35 sampling plots measured over the study area. Single trees were automatically identified
 150 and segmented using a well-established approach. AGB was estimated using the AGB~VPFs model
 151 created in phase 1. Finally, the estimated values of different procedures were compared for evaluation.

152

153 2.2. Benchmark: single tree QSM to quantify volume and AGB

154 The workflow combines both manual and automatic steps. In the first phase (see Figure 2), Trimble
 155 Real Works software (TRW) was used for tree segmentation and QSM production. Each segmented

156 tree was then reconstructed through a semi-automatic cylinder-fitting procedure, resembling the
157 traditional approach based on Smalian method for stem volume estimates, using virtual cylinders of
158 about 1 m in length. The total tree volume (V_{tree} , in m^3) was computed by summing all the cylinders
159 and then converted to biomass using Equation 1:

$$160 \quad AGB_{tree} = V_{tree} \cdot BEF \cdot WBD \quad (1)$$

161 where BEF is the Biomass Expansion Factor, used to expand growing stock volume to the aboveground
162 woody biomass volume, and WBD is the Wood Basal Density, used to convert fresh volume to dry
163 weight ($Mg\ m^{-3}$). For beech trees in central Italy $BEF_{Beech} = 1.36$ and $WBD_{Beech} = 0.61$ (Marino et al.
164 2021, Table A2).

165 For each tree, different architectural traits were also measured: (1) total tree height (TH); (2) the
166 surface of the crown at its maximum extension, considered as the crown projection ($CrPrj$); (3) and the
167 crown volume ($CrVol$). A set of algorithms was developed using functions from lidR package (Roussel
168 et al. 2020) to characterize crown features from the xyz-data of each focal tree and its neighbors. First,
169 the original point cloud of each tree was voxelised at a resolution of 25 cm, for a balance between
170 achieving suitable results and minimising computation time. To avoid residual noise in the original
171 point cloud, only voxels containing at least three points were classified as “vegetation” and used to
172 compute single-tree vertical profiles. From the smoothed curve (red-line in Figure 2), the height of the
173 maximum crown projection (Z-peak, in meters), crown base height (Z-peak-start, in meters) and total
174 tree height (Z-peak-end, in meters) were derived. Crown volume ($CrVol$) was computed as the sum of
175 all vegetation voxels between Z-peak-start and Z-peak-end, while crown projected area ($CrPrj$) was
176 determined using a 2D convex hull at the maximum crown projection. All these features were
177 identified by analysing the single-tree vertical profile with the findpeaks function from the pracma R-
178 package.

179 **2.3. AGB allometric modelling approach**

180 Following a strengthened procedure (He et al. 2018), the general biomass equation for each tree is
181 defined as:

$$182 \quad Y = \alpha X^\beta \quad (2)$$

183 where Y represents AGB and X is a correlated tree attribute, typically the dbh. In this study, X
184 corresponds to one of the considered crown features (i.e. crown projection or crown volume). To

185 address the heteroscedasticity often present in nonlinear regressions with original scales of
186 measurements (Packard, Birchard, and Boardman 2010), the Equation 2 was log transformed:

187
$$\ln(Y) = \alpha_1 + \beta_1 \ln(X) \quad (3)$$

188 AGB of an individual tree was modeled as a function of both crown projected area (*CrPrj*) and crown
189 volume (*CrVol*) of the tree, expressed as:

190
$$\ln(AGB_{CrPrj}) = \alpha_{CrPrj} + \beta_{CrPrj} \ln(CrPrj) \quad (4)$$

191
$$\ln(AGB_{CrVol}) = \alpha_{CrVol} + \beta_{CrVol} \ln(CrVol) \quad (5)$$

192 The log-transformation, however, introduced a systematic bias, typically corrected using the following
193 correction factor (CF):

194
$$CF = \exp(SEE^2/2) \quad (6)$$

195 where CF is the correction factor, and SEE is the standard error of the estimate, calculated as follows:

196
$$SEE = \sqrt{\sum_{i=1}^n (\ln(Y_i) - \ln(\hat{Y}_i))^2 / (n-2)} \quad (7)$$

197 The final equation for estimating AGB is:

198
$$AGB = e^\alpha X^\beta CF \quad (8)$$

199 where *X* is either crown projection or crown volume.

200 **2.4. Automatic ITS from ALS and UAV-LS point clouds**

201 After the first phase focused on the calibration of AGB modelling using manually measured trees, the
202 second phase tested the performance of automatic algorithms for Individual Tree Segmentation (ITS) in
203 structurally homogeneous broadleaf temperate forests. Cao et al. (2023) recently reviewed ITS methods
204 for broadleaf tropical forests - with a heterogeneous forest structure, from which Li et al. (2012)
205 method was selected for this study. This rule-based ITS algorithm, integrated into the lidR processing
206 packages (Roussel et al. 2020) offers a low cost-benefit ratio in the forest stands measured. Moreover,
207 rather than relying on raster CHM, which limits detection to dominant trees, Li et al. (2012) analyses
208 point cloud structures and has shown a detection accuracy rate of up to 90% in mixed forests. The same

209 workflow was applied to both UAV-LS and ALS data for comparison (Figure 2). To avoid time-
210 consuming procedures, specific and fixed parameters were established in the ITS algorithm.

211 2.5. Statistical analysis

212 In the first phase (Figure 2), the two previously presented models (Equation 4 and Equation 5) were
213 evaluated using data from 320 manually segmented beech trees, from the 12 sampling plots (Figure
214 FS1). AIC was used as a validation technique to assess model performance with new data. Finally, to
215 evaluate the accuracy of AGB estimates at the plot level, observed and modelled results from the same
216 12 sampling plots were compared. Model assessment metrics included R^2 and $RMSE$ computed using
217 Equation 9 as follows:

$$218 \quad RMSE = \sqrt{\frac{\sum_{i=1}^n [\ln(Y_i) - \ln(\hat{Y}_i)]^2}{n}} \quad (9)$$

219 The second phase (Figure 2) evaluated the performance of the selected ITS algorithm (Li et al. 2012)
220 for individual tree identification and crown feature extraction aimed at AGB estimation, using ALS or
221 UAV-LS data separately. Tree mapping evaluation was also conducted using completeness and
222 correctness (Laino et al. 2024). Finally, the performance of the proposed models was assessed using
223 data extrapolated from the fully automated ITC and crown featuring methods.

224 3. Results

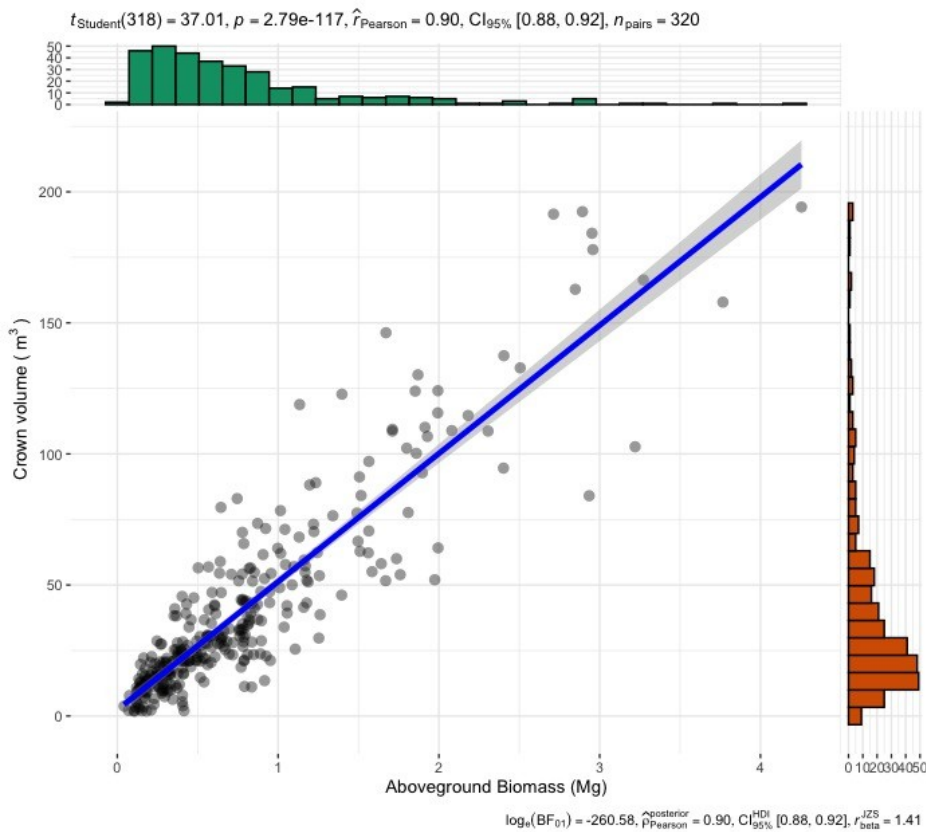
225 3.1. Phase 1: Crown features

226 The process of crown feature extraction (projection and volume) was effective over the 320 manually
227 segmented reference trees. The beta coefficient ($\beta_{CrVol}=0.78$) obtained from the best model
228 (Equation 5) representing the metabolic scaling coefficient aligns closely with the theoretical value
229 equal to 0.75. The 12 sampling plots show significant variability in the crown sizes of the trees. The
230 average crown area is 15.4 m² (min = 0.2, max = 75.7) with a standard deviation of 13.5 m², while
231 crown volume has an average of 39.9 m³ (min = 1.8, max = 194.2) with a standard deviation of 36.4
232 (Figure FS2). Pearson correlation coefficients (r) between crown features and traditional tree attributes,
233 such as dbh and total tree height, are consistently below 0.45. However, correlations increase

234 significantly to 0.88 and 0.90 when comparing tree volume with crown projection and crown volume,
235 respectively.

236 3.2. Phase 1: AGB model assessment

237 The AIC used for tree-level model assessment indicates that the model from Equation 5 (AIC=364.4)
238 performs slightly better than that from Equation 4 (AIC=397.9). Although a lower AIC (92.3) is
239 achievable using both *CrPrj* and *CrVol*, the model with *CrVol* as the sole predictor was preferred for
240 simplicity. Using *CrVol* as the predictor (Equation 5) we obtained the best result ($R^2 = 0.74$, RMSE =
241 0.41, RMSE% = 2.9 %, Figure 3).



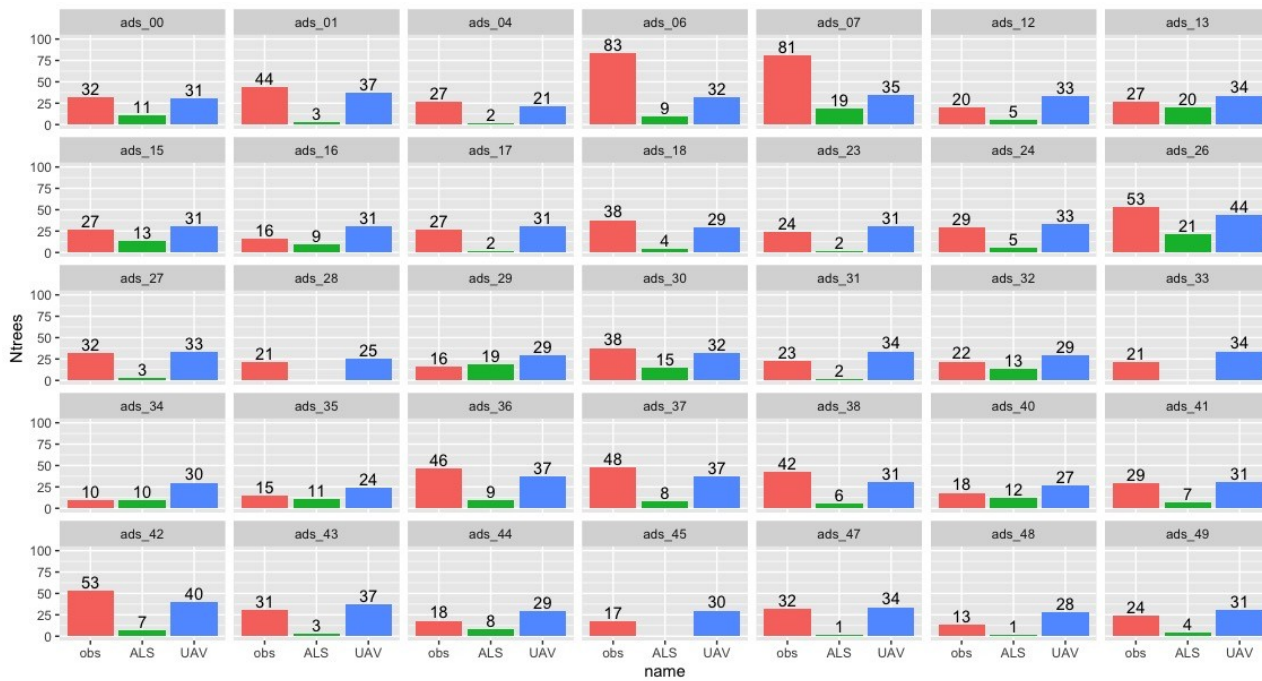
242
243 Figure 3: Scatterplot and relations between crown volume and aboveground biomass of the 320
244 sampled trees.

245

246 3.3. Phase 2: individual tree detection

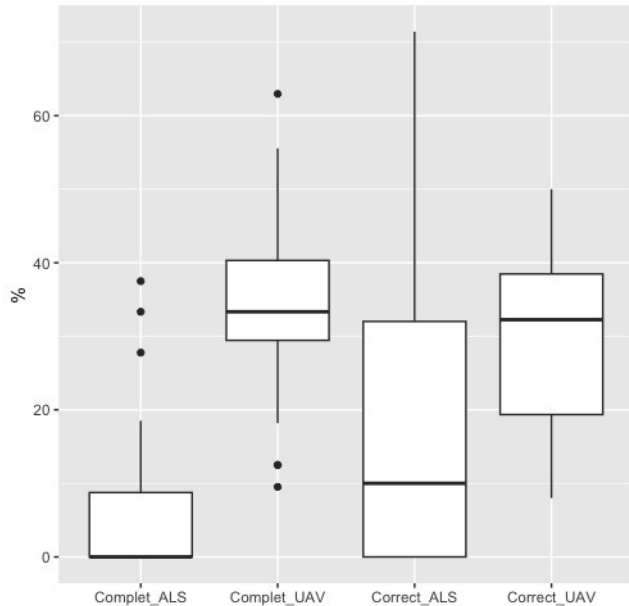
247 Figure 4 (together with Table TS1 and Figure FS3, see supplementary materials) displays results for
248 both ALS and UAV-LS individual tree detection. Under the given conditions, ALS proved to be less

249 effective, consistently performing worse than UAV-LS. ALS fails to detect many trees in several cases
 250 (3 out of 35 plots). On the other hand, UAV-LS tends to overestimate tree numbers in less dense forests
 251 and underestimate in denser forest conditions (Figure 4). The indices used for ITD assessment
 252 (completeness and correctness) exhibit similar patterns, with UAV-LS also showing better
 253 performances (Figure 5).



254
 255 Figure 4: Number of trees observed over 35 plots and estimated using both ALS and UAV point clouds
 256 by automatic segmentation.

257



258

259 Figure 5: Distributions of completeness and correctness over 35 plots from both ALS and UAV data.

260

261 Phase 2: AGB estimates from ALS and UAV-LS

262 Figure 1 shows the results of the fully automatic procedure in estimating AGB under the given

263 conditions. Using the crown surface area and the model from phase 1 (Equation 4), UAV-LS

264 consistently overestimates AGB with a relatively constant coefficient. On the other hand, ALS always

265 underestimates AGB without any clear pattern. When applying the model from Equation 5, ALS results

266 remain less accurate, while UAV-LS data produced more reliable results Figure 1.

267 4. Discussion

268 This study demonstrates that tree architectural traits (Dorji et al. 2019) influence the accuracy of AGB

269 estimates from ALS and UAV-LS, regardless of forest mixture or structure, as previously noted in

270 ground-based studies (Penanhoat et al. 2024; Pretzsch 2021).

271 Despite the homogeneous nature of the beech forests studied, there was significant variability in the

272 crown sizes of the trees we examined, with standard deviations of 13.5 m² for crown area and 36.4 m³

273 for crown volume. Reference tree crown dimensions from TLS and UAV-LS are manually defined in

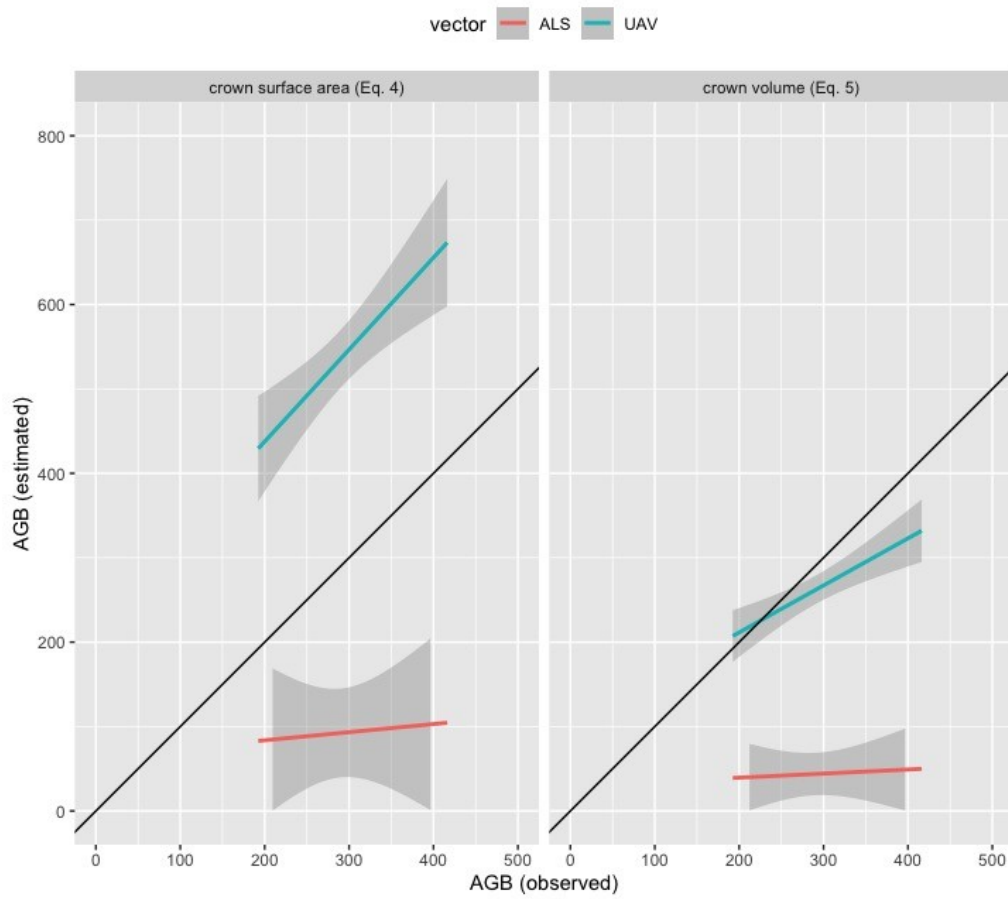
274 CloudCompare, ensuring a realistic representation of 320 standing trees for TLS and 1000 for UAV-LS

275 systems (Barbeito et al. 2017). These segmented trees were modelled using MST allometries (Li et al.
276 2012; Pretzsch and Dieler 2012).

277 When UAV-LS was analysed using the ITS algorithm developed by Li et al. (2012) dominated trees
278 were barely detected, achieving only moderate correctness and completeness (~30% for UAV-LS
279 compared to <10% for ALS).). For correctly segmented trees, crown height variability is captured by
280 analysing the 3D vertical uniformity distribution (thresholds at the 75th and 95th percentiles) (Nicola
281 Puletti et al. 2024). However, the phenotypic plasticity and deliquescent architecture of beech trees
282 affected the crown-boundary delineation of standing trees in ALS and UAV-LS point clouds, impacting
283 the AGB estimation accuracy, as noted in previous studies (Y. Wang et al. 2016). Secondary factors
284 affecting detection include forest stand characteristics (i.e., tree density: maximum 1,174 trees ha⁻¹)
285 and competition (Barbeito et al. 2017; Nicola Puletti et al. 2024); individual tree architecture (i.e.,
286 deliquescent architecture and plasticity in growth forms) (Pretzsch 2021), and technical aspects such as
287 point cloud occlusion (Alvites et al. 2021; Bruggisser et al. 2019). Following previous classifications
288 (Liang et al. 2018; Y. Wang et al. 2016), the selected forest sites fall into the moderate-to-difficult
289 complexity forest category (~443 trees ha⁻¹).

290 High-resolution TLS point clouds enable accurate tree architectural traits reconstruction (*CrVol*,
291 *CrPrj*), aligning closely with AGB estimates in the MST-based allometry model (RMSE% = 2.9%).
292 The MST model produced an acceptable beta coefficient for AGB estimates (equal to 0.78) (Lin et al.
293 2013). However, UAV-LS produces more accurate AGB estimates than ALS (Figure 6), likely due to
294 point quality captured by UAV-LS systems, allowing occlusion handling through penetration and
295 closer proximity to the top canopy (Bruggisser et al. 2019). Considering that all forest sites (except
296 ads_26; Figure 7) exhibit mono-layered vertical stratification, the primary factor probably affecting the
297 tree AGB estimation is occlusion caused by large branches overlapping smaller ones, worsened by the
298 incorrect segmentation of nearby crowns. The incorrect tree segmentation in pure stands is implicit in
299 ITS analysis, especially in the closed-canopy broadleaf stands (Barbeito et al. 2017; Cao et al. 2023).
300 Previous studies show that ALS-based crown segmentation algorithms achieve accuracies below 30%
301 for Commission I (extra trees detected within crowns) and less than 40% for Commission II (trees
302 detected outside crowns) (Y. Wang et al. 2016). Nevertheless, the tree detection method we used (Li et
303 al. 2012) achieved an F-score of 0.5 in mixed conifer forests (Pirotti, Paterno, and Pividori 2020) and a
304 75% detection rate in mixed conifer-broadleaf forests (Torresan et al. 2020), which aligns with our

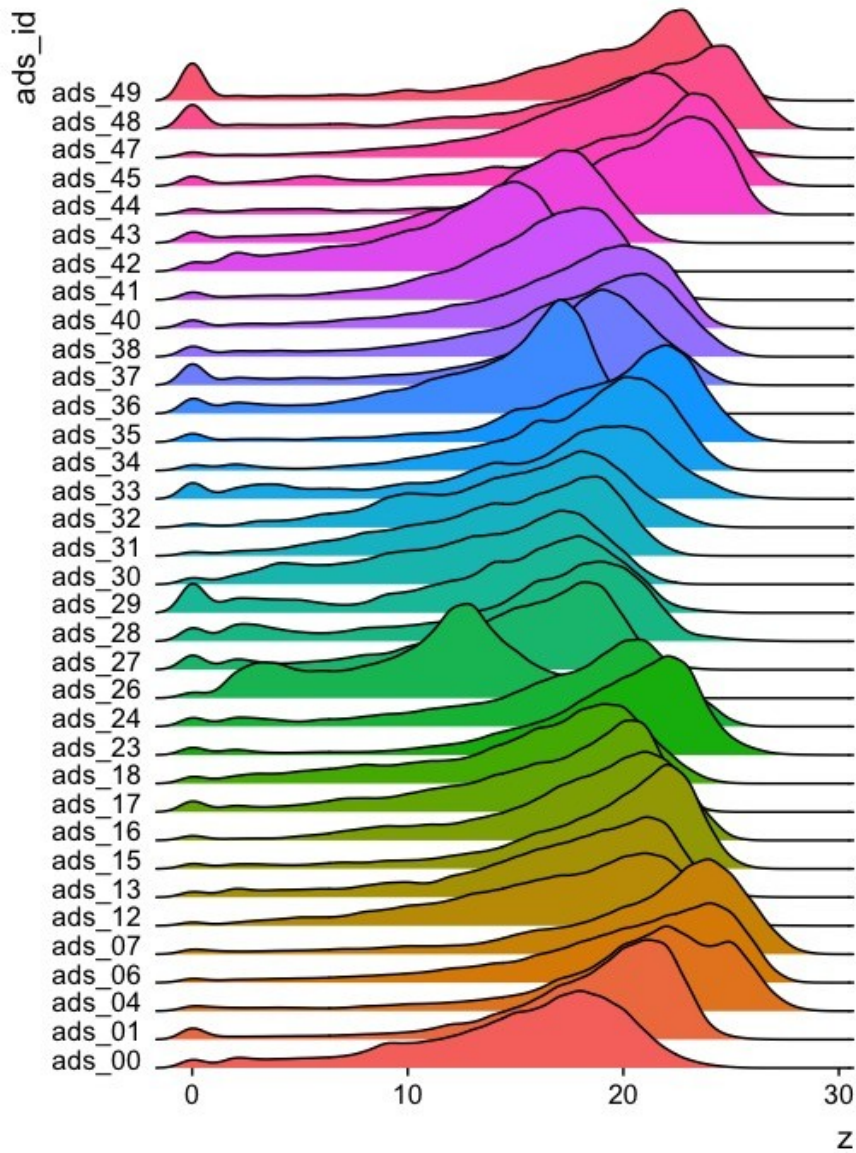
305 findings. Another challenge in tree detection was the configuration of parameters for 3D forest site
306 analysis, which was time-intensive and site-specific (Li et al. 2012).



307

308 Figure 6: Estimated AGB by both Equation 4 and 5 and with different LiDAR vectors (ALS (red) and
309 UAV-LS (green)).

310



311

312 Figure 7: Vertical profiles of 35 sampling plots, as derived from UAV-LS point clouds. With few exceptions (e.g. ads_26),
 313 the distribution is unimodal from the ground to the top of the canopy.

314

315 In this regard, unsupervised algorithms such as DBSCAN (Density-Based Spatial Clustering of
 316 Applications with Noise) (Alvites et al. 2021), hierarchical filtering and clustering (HFC) (Zhang et al.
 317 2024), or learning algorithms (i.e., convolutional neural network) (Straker et al. 2023) could prove
 318 more effective in detecting trees. However, the unavailability of these ITC algorithms in R software
 319 limits their accessibility for non-expert users. Therefore, developing R packages to integrate these
 320 advanced algorithms would be essential for expanding their use in tree detection. AI-based approaches
 321 hold promise for future tree detection and segmentation tasks. Once these challenges are addressed,

322 UAV-LS data could enable more frequent, cost-effective updates for AGB monitoring with high
323 resolution (Fassnacht et al. 2024).

324 Accurately delineating tree architectural traits can significantly affect the accuracy of AGB estimates
325 from aerial LiDAR systems, especially ALS. As expected, segmenting dominated trees remains a
326 primary challenge in our workflow; however, our findings align closely with previous studies (Liang et
327 al. 2018; Y. Wang et al. 2016). Nevertheless, the manually segmented reference trees in Phase 1
328 provided a robust validation step for the outputs in Phase 2, thanks to the detailed representation of
329 forest plots using point clouds. Integrating aerial with terrestrial LiDAR data may improve detection
330 rates, allowing closer alignment with reference AGB estimates (Alvites et al. 2022). Implementing the
331 MST to beech trees to capture crown irregularities, regardless of purity (Barbeito et al. 2017), requires
332 high-resolution point clouds, which currently limits its application to terrestrial and drone-based
333 LiDAR systems (Barbeito et al. 2017; Owen, Flynn, and Lines 2021; Martin-Ducup et al. 2020).

334 **5. Conclusions**

335 Quantifying forest aboveground biomass is crucial for climate action and forest management policies.
336 This study confirms that UAV-LS systems, with their high-density point clouds, significantly improve
337 local AGB predictions in homogeneous beech forests compared to ALS. Applying the Metabolic
338 Scaling Theory to beech trees effectively requires high-resolution point clouds, ideally from drone-
339 based LiDAR systems. Although segmenting dominated trees remains challenging, traditional crown
340 measurement methods are time-intensive and prone to errors. Integrating terrestrial and UAV-LiDAR
341 data offers an efficient and promising alternative for accurately capturing tree architecture. These
342 findings underscore the value of UAV-LS data for AGB estimation and demonstrate the potential of
343 precise crown measurements to advance climate and forestry goals.

344

345 **References**

- 346 Alvites, Cesar, Marco Marchetti, Bruno Lasserre, and Giovanni Santopuoli. 2022. "LiDAR as a Tool
347 for Assessing Timber Assortments: A Systematic Literature Review." *Remote Sensing* 14 (18): 4466.
348 <https://doi.org/10.3390/rs14184466>.
- 349 Alvites, Cesar, Giovanni Santopuoli, Mauro Maesano, Gherardo Chirici, Federico Valerio Moresi,
350 Roberto Tognetti, Marco Marchetti, and Bruno Lasserre. 2021. "Unsupervised Algorithms to Detect
351 Single Trees in a Mixed-Species and Multilayered Mediterranean Forest Using LiDAR Data."
352 *Canadian Journal of Forest Research* 51 (12): 1766–80. <https://doi.org/10.1139/cjfr-2020-0510>.

- 353 Barbeito, Ignacio, Mathieu Dassot, Dominik Bayer, Catherine Collet, Lars Drössler, Magnus Löf,
354 Miren Del Rio, et al. 2017. “Terrestrial Laser Scanning Reveals Differences in Crown Structure of
355 *Fagus Sylvatica* in Mixed Vs. Pure European Forests.” *Forest Ecology and Management* 405
356 (December): 381–90. <https://doi.org/10.1016/j.foreco.2017.09.043>.
- 357 Brede, Benjamin, Kim Calders, Alvaro Lau, Pasi Raunonen, Harm M. Bartholomeus, Martin Herold,
358 and Lammert Kooistra. 2019. “Non-Destructive Tree Volume Estimation Through Quantitative
359 Structure Modelling: Comparing UAV Laser Scanning with Terrestrial LIDAR.” *Remote Sensing of*
360 *Environment* 233 (November): 111355. <https://doi.org/10.1016/j.rse.2019.111355>.
- 361 Brede, Benjamin, Louise Terry, Nicolas Barbier, Harm M. Bartholomeus, Renée Bartolo, Kim
362 Calders, Géraldine Derroire, et al. 2022. “Non-Destructive Estimation of Individual Tree Biomass:
363 Allometric Models, Terrestrial and UAV Laser Scanning.” *Remote Sensing of Environment* 280
364 (October): 113180. <https://doi.org/10.1016/j.rse.2022.113180>.
- 365 Brosofske, Kimberley D., Robert E. Froese, Michael J. Falkowski, and Asim Banskota. 2014. “A
366 Review of Methods for Mapping and Prediction of Inventory Attributes for Operational Forest
367 Management.” *Forest Science* 60 (4): 733–56. <https://doi.org/10.5849/forsci.12-134>.
- 368 Bruggisser, M., M. Hollaus, D. Kükenbrink, and N. Pfeifer. 2019. “COMPARISON OF FOREST
369 STRUCTURE METRICS DERIVED FROM UAV LIDAR AND ALS DATA.” *ISPRS Annals of the*
370 *Photogrammetry, Remote Sensing and Spatial Information Sciences* IV-2/W5 (May): 325–32.
371 <https://doi.org/10.5194/isprs-annals-IV-2-W5-325-2019>.
- 372 Calders, Kim, Glenn Newnham, Andrew Burt, Simon Murphy, Pasi Raunonen, Martin Herold, Darius
373 Culvenor, et al. 2015. “Nondestructive Estimates of Above-Ground Biomass Using Terrestrial Laser
374 Scanning.” Edited by Sean McMahon. *Methods in Ecology and Evolution* 6 (2): 198–208.
375 <https://doi.org/10.1111/2041-210X.12301>.
- 376 Calders, Kim, Hans Verbeeck, Andrew Burt, Niall Origo, Joanne Nightingale, Yadvinder Malhi, Phil
377 Wilkes, Pasi Raunonen, Robert G. H. Bunce, and Mathias Disney. 2022. “Laser Scanning Reveals
378 Potential Underestimation of Biomass Carbon in Temperate Forest.” *Ecological Solutions and*
379 *Evidence* 3 (4). <https://doi.org/10.1002/2688-8319.12197>.
- 380 Cao, Yujie, James G. C. Ball, David A. Coomes, Leon Steinmeier, Nikolai Knapp, Phil Wilkes,
381 Mathias Disney, et al. 2023. “Benchmarking Airborne Laser Scanning Tree Segmentation Algorithms
382 in Broadleaf Forests Shows High Accuracy Only for Canopy Trees.” *International Journal of Applied*
383 *Earth Observation and Geoinformation* 123 (September): 103490.
384 <https://doi.org/10.1016/j.jag.2023.103490>.
- 385 Chirici, Gherardo, Francesca Giannetti, Ronald E. McRoberts, Davide Travaglini, Matteo Pecchi, Fabio
386 Maselli, Marta Chiesi, and Piermaria Corona. 2020. “Wall-to-Wall Spatial Prediction of Growing Stock
387 Volume Based on Italian National Forest Inventory Plots and Remotely Sensed Data.” *International*
388 *Journal of Applied Earth Observation and Geoinformation* 84 (February): 101959.
389 <https://doi.org/10.1016/j.jag.2019.101959>.
- 390 Diara, Filippo, and Marco Roggero. 2022. “Quality Assessment of DJI Zenmuse L1 and P1 LiDAR and
391 Photogrammetric Systems: Metric and Statistics Analysis with the Integration of Trimble SX10 Data.”
392 *Geomatics* 2 (3): 254–81. <https://doi.org/10.3390/geomatics2030015>.

- 393 Dorji, Yonten, Peter Annighöfer, Christian Ammer, and Dominik Seidel. 2019. “Response of Beech
394 (*Fagus Sylvatica* L.) Trees to Competition New Insights from Using Fractal Analysis.” *Remote Sensing*
395 11 (22): 2656. <https://doi.org/10.3390/rs11222656>.
- 396 Fassnacht, Fabian Ewald, Christoph Mager, Lars T Waser, Urša Kanjir, Jannika Schäfer, Ana Potočnik
397 Buhvald, Elham Shafeian, et al. 2024. “Forest Practitioners’ Requirements for Remote Sensing-Based
398 Canopy Height, Wood-Volume, Tree Species, and Disturbance Products.” Edited by Stephen Wyatt.
399 *Forestry: An International Journal of Forest Research*, May, cpae021.
400 <https://doi.org/10.1093/forestry/cpae021>.
- 401 Georgi, Louis, Matthias Kunz, Andreas Fichtner, Werner Härdtle, Karl Friedrich Reich, Knut Sturm,
402 Torsten Welle, and Goddert Von Oheimb. 2018. “Long-Term Abandonment of Forest Management
403 Has a Strong Impact on Tree Morphology and Wood Volume Allocation Pattern of European Beech
404 (*Fagus Sylvatica* L.)” *Forests* 9 (11): 704. <https://doi.org/10.3390/f9110704>.
- 405 GPL software. 2021. *GPL Software, 2021. Cloud Compare. GPL Software*.
406 <https://www.cloudcompare.org/presentation.html>.
- 407 He, Huaijiang, Chunyu Zhang, Xiuhai Zhao, Folega Foussemi, Jinsong Wang, Haijun Dai, Song Yang,
408 and Qiang Zuo. 2018. “Allometric Biomass Equations for 12 Tree Species in Coniferous and
409 Broadleaved Mixed Forests, Northeastern China.” Edited by Dusan Gomory. *PLOS ONE* 13 (1):
410 e0186226. <https://doi.org/10.1371/journal.pone.0186226>.
- 411 Heinrich, Viola H. A., Ricardo Dalagnol, Henrique L. G. Cassol, Thais M. Rosan, Catherine Torres De
412 Almeida, Celso H. L. Silva Junior, Wesley A. Campanharo, et al. 2021. “Large Carbon Sink Potential
413 of Secondary Forests in the Brazilian Amazon to Mitigate Climate Change.” *Nature Communications*
414 12 (1): 1785. <https://doi.org/10.1038/s41467-021-22050-1>.
- 415 Laino, Diego, Carlos Cabo, Covadonga Prendes, Romain Janvier, Celestino Ordonez, Tadas
416 Nikonovas, Stefan Doerr, and Cristina Santin. 2024. “3DFin: A Software for Automated 3D Forest
417 Inventories from Terrestrial Point Clouds.” Edited by Fabian Fassnacht. *Forestry: An International*
418 *Journal of Forest Research* 97 (4): 479–96. <https://doi.org/10.1093/forestry/cpae020>.
- 419 Li, Wenkai, Qinghua Guo, Marek K. Jakubowski, and Maggi Kelly. 2012. “A New Method for
420 Segmenting Individual Trees from the Lidar Point Cloud.” *Photogrammetric Engineering and Remote*
421 *Sensing* 78 (1): 75–84. <https://doi.org/10.14358/PERS.78.1.75>.
- 422 Liang, Xinlian, Juha Hyypä, Harri Kaartinen, Matti Lehtomäki, Jiri Pyörälä, Norbert Pfeifer, Markus
423 Holopainen, et al. 2018. “International Benchmarking of Terrestrial Laser Scanning Approaches for
424 Forest Inventories.” *ISPRS Journal of Photogrammetry and Remote Sensing* 144 (October): 137–79.
425 <https://doi.org/10.1016/j.isprsjprs.2018.06.021>.
- 426 Lin, Yue, Uta Berger, Volker Grimm, Franka Huth, and Jacob Weiner. 2013. “Plant Interactions Alter
427 the Predictions of Metabolic Scaling Theory.” Edited by Andrew Hector. *PLoS ONE* 8 (2): e57612.
428 <https://doi.org/10.1371/journal.pone.0057612>.
- 429 Marino, Davide, Margherita Palmieri, Angelo Marucci, and Massimo Tufano. 2021. “Comparison
430 Between Demand and Supply of Some Ecosystem Services in National Parks: A Spatial Analysis
431 Conducted Using Italian Case Studies.” *Conservation* 1 (1): 36–57.
432 <https://doi.org/10.3390/conservation1010004>.

433 Martin-Ducup, Olivier, Pierre Ploton, Nicolas Barbier, Stéphane Momo Takoudjou, Gislain Mofack,
434 Narcisse Guy Kamdem, Thierry Fourcaud, Bonaventure Sonké, Pierre Couteron, and Raphaël Pélissier.
435 2020. “Terrestrial Laser Scanning Reveals Convergence of Tree Architecture with Increasingly
436 Dominant Crown Canopy Position.” Edited by Mark Tjoelker. *Functional Ecology* 34 (12): 2442–52.
437 <https://doi.org/10.1111/1365-2435.13678>.

438 Næsset, Erik. 2004. “Practical Large-Scale Forest Stand Inventory Using a Small-Footprint Airborne
439 Scanning Laser.” *Scandinavian Journal of Forest Research* 19 (2): 164–79.
440 <https://doi.org/10.1080/02827580310019257>.

441 Owen, Harry J. F., William R. M. Flynn, and Emily R. Lines. 2021. “Competitive Drivers of
442 Interspecific Deviations of Crown Morphology from Theoretical Predictions Measured with Terrestrial
443 Laser Scanning.” *Journal of Ecology* 109 (7): 2612–28. <https://doi.org/10.1111/1365-2745.13670>.

444 Packard, Gary C., Geoffrey F. Birchard, and Thomas J. Boardman. 2010. “Fitting Statistical Models in
445 Bivariate Allometry.” *Biological Reviews* 86 (3): 549–63. <https://doi.org/10.1111/j.1469-185x.2010.00160.x>.

447 Penanhoat, Alice, Nathaly Guerrero Ramirez, Méline Aubry-Kientz, Lucas Diekmann, Sharath Paligi,
448 Michela Audisio, Klara Mrak, and Dominik Seidel. 2024. “Effect of Competition Intensity and
449 Neighbor Identity on Architectural Traits of *Fagus Sylvatica*.” *Trees* 38 (5): 1177–87.
450 <https://doi.org/10.1007/s00468-024-02544-3>.

451 Pirotti, F., C. Paterno, and M. Pividori. 2020. “APPLICATION OF TREE DETECTION METHODS
452 OVER LIDAR DATA FOR FOREST VOLUME ESTIMATION.” *The International Archives of the
453 Photogrammetry, Remote Sensing and Spatial Information Sciences* XLIII-B3-2020 (August): 1055–
454 60. <https://doi.org/10.5194/isprs-archives-XLIII-B3-2020-1055-2020>.

455 Ploton, Pierre, Frédéric Mortier, Maxime Réjou-Méchain, Nicolas Barbier, Nicolas Picard, Vivien
456 Rossi, Carsten Dormann, et al. 2020. “Spatial Validation Reveals Poor Predictive Performance of
457 Large-Scale Ecological Mapping Models.” *Nature Communications* 11 (1): 4540.
458 <https://doi.org/10.1038/s41467-020-18321-y>.

459 Pretzsch, Hans. 2021. “Tree Growth as Affected by Stem and Crown Structure.” *Trees* 35 (3): 947–60.
460 <https://doi.org/10.1007/s00468-021-02092-0>.

461 Pretzsch, Hans, and Jochen Dieler. 2012. “Evidence of Variant Intra- and Interspecific Scaling of Tree
462 Crown Structure and Relevance for Allometric Theory.” *Oecologia* 169 (3): 637–49.
463 <https://doi.org/10.1007/s00442-011-2240-5>.

464 Puletti, N., M. Grotti, C. Ferrara, and F. Chianucci. 2020. “Lidar-Based Estimates of Aboveground
465 Biomass Through Ground, Aerial, and Satellite Observation: A Case Study in a Mediterranean Forest.”
466 *Journal of Applied Remote Sensing* 14 (4). <https://doi.org/10.1117/1.JRS.14.044501>.

467 Puletti, Nicola, Matteo Guasti, Simone Innocenti, Lorenzo Cesaretti, and Ugo Chiavetta. 2024. “A
468 Semi-Automatic Approach for Tree Crown Competition Indices Assessment From UAV LiDAR.”
469 *Remote Sensing* 16 (14): 2576. <https://doi.org/10.3390/rs16142576>.

470 Puletti, Nicola, Simone Innocenti, and Matteo Guasti. 2024. “A co-registration approach between
471 terrestrial and UAV laser scanning point clouds based on ground and trees features.” *Annals of
472 Silvicultural Research* 49 (2). <https://doi.org/10.12899/asr-2513>.

473 Roussel, Jean-Romain, David Auty, Nicholas C. Coops, Piotr Tompalski, Tristan R. H. Goodbody,
474 Andrew Sánchez Meador, Jean-François Bourdon, Florian De Boissieu, and Alexis Achim. 2020.
475 “lidR: An R Package for Analysis of Airborne Laser Scanning (ALS) Data.” *Remote Sensing of*
476 *Environment* 251 (December): 112061. <https://doi.org/10.1016/j.rse.2020.112061>.

477 Shao, Gang, Songlin Fei, and Guofan Shao. 2023. “A Robust Stepwise Clustering Approach to Detect
478 Individual Trees in Temperate Hardwood Plantations Using Airborne LiDAR Data.” *Remote Sensing*
479 15 (5): 1241. <https://doi.org/10.3390/rs15051241>.

480 Shao, Gang, Guofan Shao, Joey Gallion, Michael R. Saunders, Jane R. Frankenberger, and Songlin Fei.
481 2018. “Improving Lidar-Based Aboveground Biomass Estimation of Temperate Hardwood Forests
482 with Varying Site Productivity.” *Remote Sensing of Environment* 204 (January): 872–82.
483 <https://doi.org/10.1016/j.rse.2017.09.011>.

484 Shao, Jie, Wei Yao, Peng Wan, Lei Luo, Puzuo Wang, Lingbo Yang, Jiaxin Lyu, and Wuming Zhang.
485 2022. “Efficient Co-Registration of UAV and Ground LiDAR Forest Point Clouds Based on Canopy
486 Shapes.” *International Journal of Applied Earth Observation and Geoinformation* 114 (November):
487 103067. <https://doi.org/10.1016/j.jag.2022.103067>.

488 Straker, Adrian, Stefano Puliti, Johannes Breidenbach, Christoph Kleinn, Grant Pearse, Rasmus Astrup,
489 and Paul Magdon. 2023. “Instance Segmentation of Individual Tree Crowns with YOLOv5: A
490 Comparison of Approaches Using the ForInstance Benchmark LiDAR Dataset.” *ISPRS Open Journal*
491 *of Photogrammetry and Remote Sensing* 9 (August): 100045.
492 <https://doi.org/10.1016/j.ophoto.2023.100045>.

493 Štroner, Martin, Rudolf Urban, and Lenka Línková. 2021. “A New Method for UAV Lidar Precision
494 Testing Used for the Evaluation of an Affordable DJI ZENMUSE L1 Scanner.” *Remote Sensing* 13
495 (23): 4811. <https://doi.org/10.3390/rs13234811>.

496 Torresan, Chiara, Andrea Berton, Federico Carotenuto, Salvatore Filippo Di Gennaro, Beniamino
497 Gioli, Alessandro Matese, Franco Miglietta, Carolina Vagnoli, Alessandro Zaldei, and Luke Wallace.
498 2017. “Forestry Applications of UAVs in Europe: A Review.” *International Journal of Remote Sensing*
499 38 (8-10): 2427–47. <https://doi.org/10.1080/01431161.2016.1252477>.

500 Torresan, Chiara, Federico Carotenuto, Ugo Chiavetta, Franco Miglietta, Alessandro Zaldei, and
501 Beniamino Gioli. 2020. “Individual Tree Crown Segmentation in Two-Layered Dense Mixed Forests
502 from UAV LiDAR Data.” *Drones* 4 (2): 10. <https://doi.org/10.3390/drones4020010>.

503 Verkerk, Pieter Johannes, Joanne Brighid Fitzgerald, Pawan Datta, Matthias Dees, Geerten Martijn
504 Hengeveld, Marcus Lindner, and Sergey Zudin. 2019. “Spatial Distribution of the Potential Forest
505 Biomass Availability in Europe.” *Forest Ecosystems* 6 (1): 5. <https://doi.org/10.1186/s40663-019-0163-5>.

507 Wang, Yunsheng, Juha Hyypä, Xinlian Liang, Harri Kaartinen, Xiaowei Yu, Eva Lindberg, Johan
508 Holmgren, et al. 2016. “International Benchmarking of the Individual Tree Detection Methods for
509 Modeling 3-d Canopy Structure for Silviculture and Forest Ecology Using Airborne Laser Scanning.”
510 *IEEE Transactions on Geoscience and Remote Sensing* 54 (9): 5011–27.
511 <https://doi.org/10.1109/TGRS.2016.2543225>.

- 512 Wang, Zhien, and Massimo Menenti. 2021. "Challenges and Opportunities in Lidar Remote Sensing."
513 *Frontiers in Remote Sensing* 2 (March): 641723. <https://doi.org/10.3389/frsen.2021.641723>.
- 514 Xu, Dandan, Haobin Wang, Weixin Xu, Zhaoqing Luan, and Xia Xu. 2021. "LiDAR Applications to
515 Estimate Forest Biomass at Individual Tree Scale: Opportunities, Challenges and Future Perspectives."
516 *Forests* 12 (5): 550. <https://doi.org/10.3390/f12050550>.
- 517 Zhang, Cailian, Chengwen Song, Aleksandra Zaforemska, Jiaying Zhang, Rachel Gaulton, Wenxia
518 Dai, and Wen Xiao. 2024. "Individual Tree Segmentation from UAS Lidar Data Based on Hierarchical
519 Filtering and Clustering." *International Journal of Digital Earth* 17 (1): 2356124.
520 <https://doi.org/10.1080/17538947.2024.2356124>.

521